Generalization of the PIV loss-of-correlation formula introduced by Keane and Adrian

Sven Scharnowski[1] · Kristian Grayson[2] · Charitha M. de Silva[2] · Nicholas Hutchins[2] · Ivan Marusic[2] · Christian J. Kähler[1]

Abstract In 2D particle image velocimetry (PIV), the loss-of-correlation due to out-of-plane motion or light-sheet mismatch has two effects. First, it reduces the probability of detecting a valid vector. Second, it increases the uncertainty measured in velocity fields. The loss-of-correlation is commonly determined by the F_O factor, which was initially proposed by Keane and Adrian (Appl Sci Res 49:191–215, 1992). However, the present study demonstrates that the validity of the original F_O definition is confined to cases with identical laser intensity profiles. As light sheets usually differ in width and shape, the proposed definition is of limited use in reality. To overcome this restriction, a new definition for F_O is proposed which covers the effect of light-sheet pairs with different shapes and widths. The proposed improvement was validated by means of synthetic PIV images based on various light-sheet profiles. The loss-of-correlation for the images was compared to the theoretical solution based on the light-sheet profiles. The results show that the new definition of F_O accurately predicts the loss-of-correlation for all tested laser mismatches and agrees with the old definition for the ideal case involving identical light sheets. Based on the revised F_O definition, prediction of loss-of-correlation due to light-sheet mismatches and misalignment is now possible using a laser profiling camera. This allows the optimization of a laser prior to any PIV measurements. For the case of out-of-plane motion, the loss-of-correlation can also be estimated from the correlation function of the PIV images. Thus, it is possible to optimize the laser alignment to match the flow conditions while setting up an experiment. These findings help experimentalists to understand and control the sources of errors associated with out-of-plane effects and help to minimize the measurement uncertainty.

✉ Sven Scharnowski
sven.scharnowski@unibw.de

Kristian Grayson
kristiangrayson@gmail.com

[1] Institute of Fluid Mechanics and Aerodynamics, Bundeswehr University Munich, Neubiberg, Germany

[2] The University of Melbourne, Victoria 3010, Australia

1 Introduction

Today, 3D measurements using PIV and PTV are becoming more and more popular, but the majority of measurements continue to use planar 2D PIV and PTV techniques. These methods are very reliable, robust, and easy to handle. Furthermore, the equipment required for these measurements is readily available to many researchers worldwide. The uncertainty of the method is also well characterized (Charonko and Vlachos 2013; Sciacchitano et al. 2015; Sciacchitano and Wieneke 2016; Timmins et al. 2012; Wieneke 2015; Xue et al. 2015; Scharnowski and Kähler 2016a; Kähler et al. 2012). This is very important, because accurate measurements together with reliable error estimations are essential for the measurement process.

Although planar PIV is generally robust, the thin light sheet can cause measurement difficulties in flows with out-of-plane components, caused by the 3D motion of the flow (turbulence) or the orientation of the light sheet with respect to the primary flow direction. In these scenarios, the tracer particles seeded in the flow move in and out of the thin measurement volume if the out-of-plane flow velocity is non-zero. A thin light sheet can also exacerbate the impact of any unintentional misalignment between the two beams of a double pulse PIV laser. However, if a constant out-of-plane motion is present, as is typical when the measurement plane is not perfectly aligned to the main flow direction, a

small adjustment to the light-sheet alignment can also be used to correct for these out-of-plane flows, as discussed in Kähler and Kompenhans (2000). This is equivalent to the window-shifting technique used in the evaluation of PIV recordings to compensate for the in-plane shift of the particle images. However, a simple shift of the light sheet cannot fully correct the effects in case of more complex, or even three-dimensional flows. The effect of out-of-plane motion on the probability of detecting a valid vector is illustrated in Fig. 1 for different numbers of particle images (N_I) within the interrogation window. The results in the figure are based on the analysis of synthetic PIV images with zero in-plane displacement, corresponding to the final pass of a multi-pass PIV evaluation.

If the correlation value in the center of the correlation plane is higher than all other peaks within a search radius, the corresponding vector is considered to be a valid one. Otherwise, if another peak is higher than the center peak, the vector is not valid. The valid detection probability is the ratio of the number of valid vectors to the total number of vectors. It can be clearly seen from Fig. 1 that out-of-plane motion or a light-sheet mismatch has a strong effect on the probability of detecting a valid vector. This is particularly true if 10 or less particle images are considered in the analysis, as typical for the final pass of an iterative PIV evaluation. If no valid vector is found during the first evaluation pass, the image deformation for the following passes cannot function correctly. Therefore, it is very important to start the multi-pass evaluation with sufficiently large interrogation windows if strong out-of-plane effects are present.

Besides the valid detection probability, out-of-plane motion also affects the shift-vector uncertainty, as illustrated in Fig. 2. The out-of-plane displacement Δz is only one parameter among many that affects the measurement uncertainty, meaning that it is not possible to determine the actual uncertainty only from the out-of-plane motion. Nevertheless, it is evident from Fig. 2 that out-of-plane motion can have a strong effect on the uncertainty. Thus, understanding the loss-of-correlation caused by out-of-plane motion can help to identify error sources and to optimize PIV setups.

Out-of-plane loss-of-particles can be reduced by increasing the light-sheet thickness and by decreasing the temporal separation between the laser pulses Δt. However, this is limited due to the following reasons: First, thickening the light sheet reduces the energy density of the laser light and causes reduced signal strength in PIV images. Second, thicker light sheets result in lower spatial resolution in the out-of-plane direction. This is especially crucial in the presence of out-of-plane gradients, such as in the wall-parallel plane of a turbulent boundary layer. Third, a small Δt results in reduced loss-of-pairs, but increases the relative measurement uncertainty and reduces the dynamic velocity range. Scharnowski and Kähler (2016a) have shown that some loss-of-pairs should be accepted for three-dimensional flows to optimize between correlation strength and shift vector length. Thus, in 3D flows, an optimum value for Δt must be found to achieve valid vectors with low uncertainty.

The present study extends the work in Scharnowski and Kähler (2016a). Its main purpose is to solve the issues related to the classical definition of F_O, as pointed out by Grayson et al. (2016). The following section summarizes the limits of the classical definition of F_O, while Sect. 3

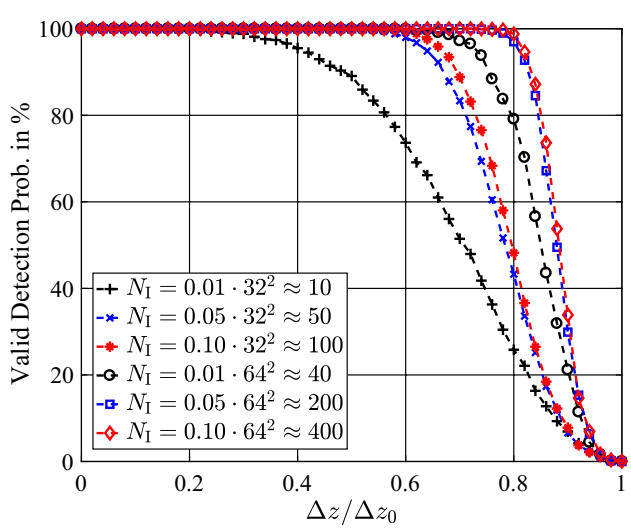

Fig. 1 Probability of detecting a valid vector from PIV measurements as a function of the out-of-plane motion Δz normalized by the light-sheet thickness Δz_0 for different particle image densities (N_{ppp} = 0.01; 0.05; 0.10) and interrogation window sizes (32^2 and 64^2 pixel). A Gaussian light-sheet shape was used in this simulation

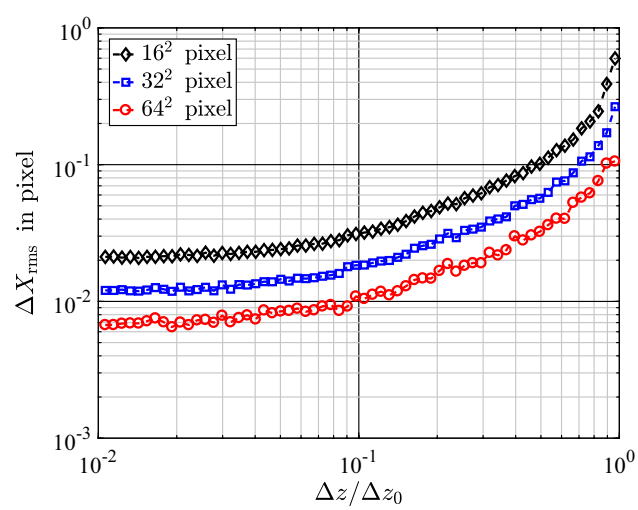

Fig. 2 Shift vector uncertainty as a function of the out-of-plane motion Δz normalized by the light-sheet thickness Δz_0 for a particle image density of N_{ppp} = 0.10 and different interrogation window sizes. The simulated light-sheet shape factor was $s_{1,2}$ = 10 (see Eq. 2)

introduces a new definition. Section 4 outlines laser optic adjustments for correcting light-sheet mismatch, assuming zero out-of-plane motion. Section 5 discusses the impacts of out-of-plane velocity on F_O, and Sect. 6 presents a method of estimating F_O from PIV images. Finally, the findings are validated experimentally in Sect. 7 using wall-parallel PIV measurements in a turbulent boundary layer.

2 The classical definition of F_O

Keane and Adrian (1992) defined the loss-of-correlation due to out-of-plane motion as follows:

$$F_{O(1992)} = \frac{\int I_1(z - z_{01}) \times I_2(z - z_{02} - \Delta z)\mathrm{d}z}{\int I_1(z) \times I_2(z)\mathrm{d}z} \tag{1}$$

where $I_{1,2}(z)$ denote the intensity of the two light-sheet profiles centered at the measurement plane, $z_{01,02}$ are the parallel offsets of the two light sheets with respect to the measurement plane, and Δz is the out-of-plane displacement of the particles. This loss-of-correlation factor estimates the reduction in correlation peak height due to out-of-plane loss-of-pair effects. $F_{O(1992)}$ equals 1 if every particle image has a corresponding partner in a PIV image pair. If some particles enter or leave the light sheet, $F_{O(1992)}$ decreases and is reduced to zero if no particle image can be paired.

To discuss Eq. (1) in more detail, the following laser light-sheet intensity profiles are used for the first and second laser pulse (I_1 and I_2, respectively).

$$I_{1,2}(z) = I_{01,02} \times \exp\left[-\frac{1}{\sqrt{2\pi}}\left|\left(\frac{2z}{\Delta z_{01,02}}\right)^{s_{1,2}}\right|\right] \tag{2}$$

The profiles are based on a Gaussian, $I_{01,02}$ are the maximum intensities in the light-sheet center, and $\Delta z_{01,02}$ are the widths at which the intensity drops to $I_{01,02} \times \exp\left(-1/\sqrt{2\pi}\right) \approx 0.67 \times I_{01,02}$. The factor $1/\sqrt{2\pi}$ ensures that the squared intensity is independent of the shape factor $s_{1,2}$ for a fixed light-sheet thickness. As a result of this, different light-sheet shapes lead to a comparable average signal level, which is characterized by the PIV image intensity standard deviation σ_A. This allows the effect of image noise for different laser profiles to be compared, as discussed in Scharnowski and Kähler (2016b). For $s_{1,2} = 2$, the intensity profiles are Gaussian, and for larger values, they become closer to a top-hat profile, as illustrated in Fig. 3. As the two laser intensity profiles $I_1(z)$ and $I_2(z)$ differ in terms of shape, width and intensity in practice, a systematic analysis of the sensitivity of the light-sheet mismatch becomes possible using Eq. (2).

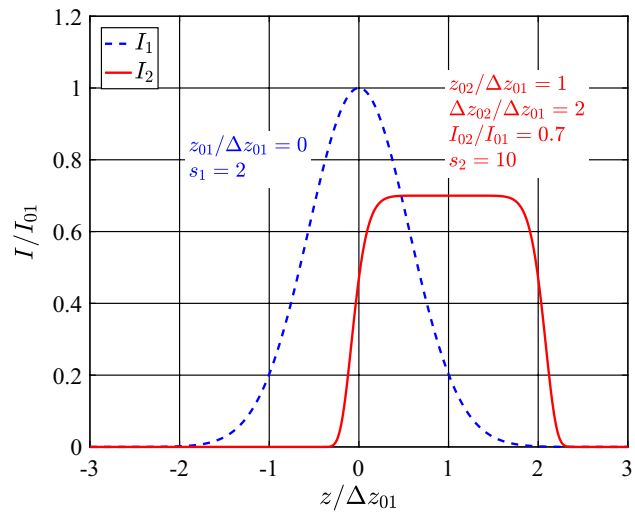

Fig. 3 Two laser light-sheet profiles generally differ in terms of shape, width, intensity, and location

Equation (1) predicts the correct loss-of-correlation if both light-sheet profiles are identical. However, it does not work in the case of different light-sheet shapes ($s_1 \neq s_2$) or widths ($\Delta z_{02} \neq \Delta z_{02}$). If, for instance, the second light sheet is twice as wide as the first one ($2\Delta z_{01} = \Delta z_{02}$), Eq. (1) results in $F_{O(1992)} = 1$ if the out-of-plane motion is fully compensated by the parallel offset between the light sheets (e.g., $z_{01} = z_{01} - \Delta z$). For this case, a significant fraction of the particle images in the second frame does not have a corresponding partners in the first frame (for top-hat profiles), or their intensity differs (for Gaussian profiles). In addition, in the case of different light-sheet shapes ($s_1 \neq s_2$), the intensity in the outer regions of the measurement plane differs for both frames, resulting in loss-of-correlation.

3 A more general definition of F_O

To account for the difference in the two light-sheet profiles, the denominator of Eq. (1) must be modified as follows:

$$F_O = \frac{\int I_1(z - z_{01}) \times I_2(z - z_{02} - \Delta z)\mathrm{d}z}{\sqrt{\int I_1^2(z)\mathrm{d}z \times \int I_2^2(z)\mathrm{d}z}} \tag{3}$$

Using the squared intensity of each of the light sheets ensures that the contribution of all particles within both profiles are considered in the same way as they are used for computing the cross-correlation function. With this new definition for the loss-of-correlation due to out-of-plane effects, F_O can now also be computed for light sheets with any combination of shape or width differences. It is important to note that Eq. (3) can be used for any arbitrary laser

profiles, although a variation of the shape factor and the width according to Eq. (2) is the focus of this section.

The effect of different shape factors on the loss-of-correlation is illustrated in Fig. 4, where the three different curves correspond to a fixed s_1 and varied s_2. The solid lines in the figure represent the theory according to Eq. (3). Besides the theoretical values, the loss-of-correlation was also computed from synthetic PIV images, indicated by the symbols.

The generation of the synthetic images follows the approach outlined in Scharnowski and Kähler (2016a). The simulated particle image diameter (4σ width of a Gaussian) was three pixels and the particle image density was set to $N_{\mathrm{ppp}} = 0.03$, if not stated otherwise. The symbols in Fig. 4 represent the maximum height of the normalized cross-correlation function computed from a zero-displacement synthetic flow without any image noise. Only in this case of zero displacement does the height of the normalized cross-correlation function equal the F_{O} factor. This approach ensures that loss-of-correlation can only occur due to out-of-plane effects, e.g., the light-sheet shape in the case of Fig. 4. The mean value and standard deviation, indicated by the error bars, were computed from the height of 100 correlation functions based on an interrogation window size of 250^2 pixel.

The good agreement between the correlation height and theoretical values confirms the value and utility of Eq. (3) for the case of different light-sheet shapes. On the other hand, the classical definition from Eq. (1) results in $F_{\mathrm{O}(1992)} = 1$ for all shape factor combinations, illustrated by the dashed line in Fig. 4. The difference between the classical and the new definition of F_{O} clearly shows that it is important to account for differences in the light-sheet shape. Combining a Gaussian and a top-hat profile, for instance, reduces the correlation height by about 10%.

The effect of different light-sheet widths on the loss-of-correlation is illustrated in Fig. 5. As before, the theoretical values according to Eq. (3) are shown together with the correlation height of synthetic images and the classical loss-of-correlation. The classical definition of $F_{\mathrm{O}(1992)}$ is not sensitive to different widths and always results in $F_{\mathrm{O}(1992)} = 1$ (the dashed line in Fig. 5).

The new approach exhibits a very different behavior: the loss-of-correlation factor is only unity if the widths are exactly identical, while $F_{\mathrm{O}} < 1$ for light sheets with different widths. If the widths differ by a factor of two, for instance, F_{O} drops to 0.71 for a top-hat profile and to 0.89 for a Gaussian, respectively. Besides identical shape factors, Fig. 5 also shows the effect of different widths on F_{O} for the case of two different profiles (Gaussian and top-hat). As expected from Fig. 4, two different shape factors never result in a perfect correlation. For this case, the highest F_{O} is reached if the top-hat profile is about 1.6 times wider than the Gaussian profile. It is important to note that this relation depends on the definition of the profiles, see Eq. (2). However, it can be stated that for PIV a difference in the light-sheet width is much more critical to good correlation than any difference in the shape of the intensity distribution, according to Figs. 4 and 5, provided that the overlap is well adjusted.

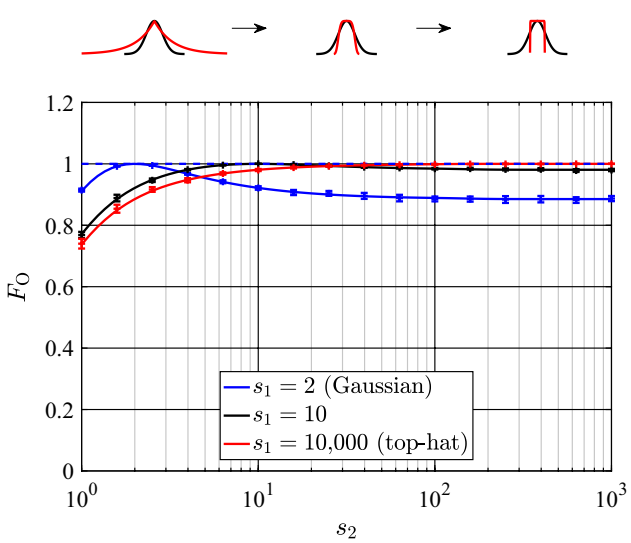

Fig. 4 Loss-of-correlation due to out-of-plane effects for light sheets with different shape factors s_1 and s_2, according to Eq. (2). The different colors correspond to different values for $s_{1,2}$. Solid lines are computed from Eq. (3), symbols represent the normalized correlation height of synthetic images, and the dashed line shows the classical $F_{\mathrm{O}(1992)}$ computed from Eq. (1)

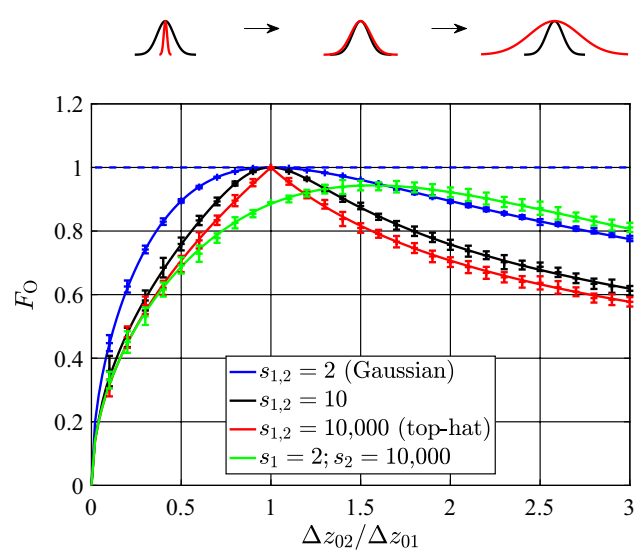

Fig. 5 Loss-of-correlation for light sheets with different widths $\Delta z_{01,02}$ shown for several shape factors $s_{1,2}$. The different colors correspond to different values for $s_{1,2}$. Solid lines are computed from Eq. (3), symbols represent the normalized correlation height of synthetic images, and the dashed line shows the classical $F_{\mathrm{O}(1992)}$ computed from Eq. (1)

Figure 6 shows the F_O factor for misaligned light sheets, e.g., a parallel offset between two identical profiles. For this case, the classical and the new definition of F_O result in the same loss-of-correlation. An exception is any case involving different shape factors, where the classical approach (dashed green line) overestimates F_O, as predicted. Figure 6 clearly shows that misaligned laser pulses can result in a dramatic reduction of the correlation strength. It is also interesting to note that the Gaussian profile is less sensitive to relatively small misalignment compared with a top-hat profile, indicated by the small slope of the blue curve close to $(\Delta z_{01} - \Delta z_{02})/\Delta z_{01} = 0$ in Fig. 6. This behavior will be discussed in more detail in Sect. 5.

4 Assessing light-sheet mismatch using F_O

Synthetic zero-displacement PIV images were used in Sect. 3 to demonstrate the effectiveness of F_O in assessing the impacts of mismatched light-sheet intensity profiles and out-of-plane velocities. It is only in this case involving zero in-plane displacement that the height of the normalized cross-correlation function is equivalent to the F_O factor. The remainder of this study focuses on the application of this metric to experimental scenarios, to assist with the refinement of a measurement configuration and improve the quality of PIV results.

Before considering the implications of out-of-plane velocity on PIV measurements, a well-matched light-sheet baseline is required. This includes ensuring similar light-sheet widths, alignment (assuming zero out-of-plane velocity), and shape factor. To perform the necessary iterative adjustments to the laser and optical configuration, several methods exist to evaluate the light-sheet overlap: a simple visual inspection in the near and far fields of the light-sheet, switching between the first and second lasers, allows for reliable optical adjustments prior to the experiment, but does not offer quantitative feedback on the adjustment quality. Imaging a surface normal to the light sheet, as it is illuminated by the laser, can extend this simple inspection to quantify the laser intensity distribution and alignment (used by Fond et al. 2015). Inclining the imaged surface can further increase the resolution of this diagnostic (employed by Kähler and Kompenhans 2000; Mistry and Dawson 2014). Burn tests offer a simple alternative (see Kähler et al. 1998 or Ganapathisubramani et al. 2005 for instance), although the limited dynamic range of burn paper can restrict its use to identifying misalignment and severe width mismatch in light sheets.

Reducing the time separation between the laser pulses to the shortest possible duration results in almost no displacement of the particles and maximizes the height of the normalized cross-correlation function. This method can be applied to experiments involving constant measurement conditions over the time required for laser adjustment. However, this approach cannot distinguish between laser light-sheet mismatch and other effects on the cross-correlation value. Furthermore, while this method may indicate a problem with the experimental setup, it does not inform changes necessary to correct this issue.

Directly measuring the light-sheet intensity profiles provides the most detailed feedback on light-sheet overlap and on F_O, calculated using Eq. (3). Furthermore, the most comprehensive and robust means of examining PIV light-sheet profiles involve the use of a laser beam profiling camera. While traditionally this type of device has been an expensive, specialized investment, often only made by a subset of experimentalists and technicians, access to laser profiling equipment no longer requires significant expense (Grayson et al. 2016). However, all of these tools can inform the corrections needed to reduce light-sheet mismatch and can offer rapid feedback on the impact of any adjustments.

The results shown in Figs. 4, 5, and 6 indicate that the matching of light-sheet width and alignment have the greatest impact on PIV measurement performance. The light-sheet thickness and offset can typically be tuned iteratively via the light-sheet optics (which applies equal width change to both light sheets), and laser system's beam combining optics, respectively, for improved F_O. However some mismatches in light-sheet width, as well as differences in shape factor, can be dictated by the fundamental beam profile behavior of each laser cavity and may be difficult to correct.

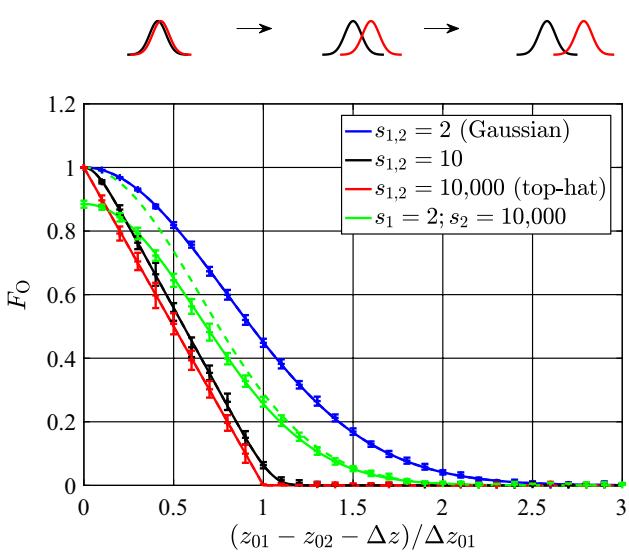

Fig. 6 Loss-of-correlation for light sheets with parallel offsets $(z_{01} - z_{02} - \Delta z)$ normalized by the light-sheet thickness Δz_{01} shown for several shape factors $s_{1,2}$. The different colors correspond to different values for $s_{1,2}$. Solid lines are computed from Eq. (3), symbols represent the normalized correlation height of synthetic images, and the dashed line shows the classical $F_{O(1992)}$ computed from Eq. (1)

While substitution of the laser system with a better performing unit may bypass these concerns, this is rarely a practical solution. Since such width and shape factor characteristics tend to vary over the spread of the light sheet, regions of superior matching in shape factor and width may be identified and aligned with the measurement field of view. This detailed examination over the full spread of the light sheet will likely require the resolution of a laser profiling camera, but such a technique can maximize the shape factor and width matching (and therefore maximizing F_O) for a given experiment.

Once the best compromise in light-sheet width and shape factor mismatch is achieved, the alignment of the light-sheet profiles can be refined and optimized, assuming zero out-of-plane motion. This involves adjusting the alignment of the two cavities of a PIV double pulse laser, using the laser's beam combining optics. Given the presence of beam pointing jitter in laser systems, which generates shot-to-shot variation in laser beam location and overlap, the light-sheet overlap should be calculated as an average from several measurements following sufficient warming of the system (see Grayson et al. 2017). Figure 7 shows various idealised examples illustrating light-sheet pairs with optimized overlap. For symmetric profiles with a single peak, as shown on the top row of the figure, the best overlap is achieved if the light-sheet centers fall on top of each other. In this case,

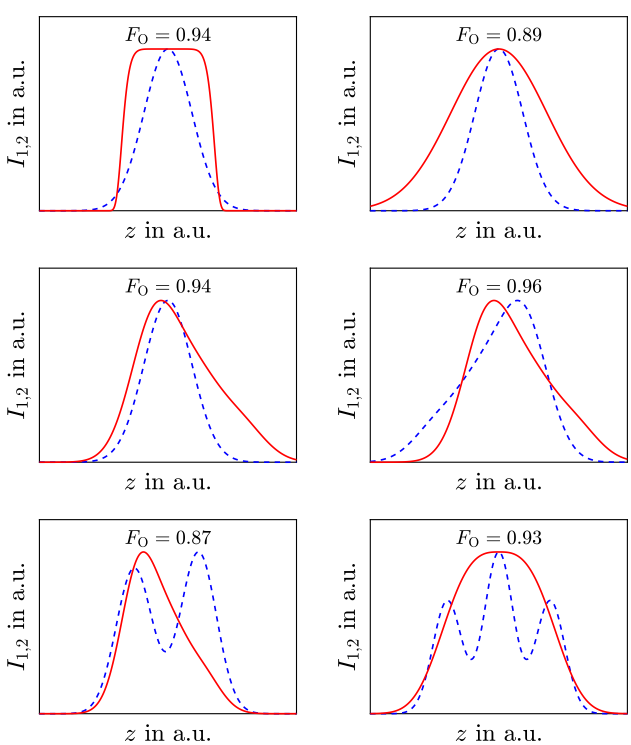

Fig. 7 Examples of different light-sheet pairs with optimized overlap. The given F_O is based on zero out-of-plane motion

the value of F_O depends mainly on the variations in shape and width. If the light-sheet profiles are skewed or contain multiple local maxima, the optimum overlap position might be less obvious, as sketched in the middle and lower row of Fig. 7. It is interesting to note that while all of the examples in Fig. 7 result in $F_O < 1$, these examples would result in $F_{O(1992)} = 1$ by following the classical definition from Eq. (1).

It is worthwhile noting that the effective width of the light sheet which directly influences correlation may not correspond to the complete profiles measured using these techniques, which alters the extent of the profiles which should strictly be considered in the F_O calculation. However, further investigation of this subject is needed, and such refinements should have only a modest effect on the resulting F_O value.

5 Impact of out-of-plane velocity

Besides the light-sheet overlap of the laser system, the particle motion in the out-of-plane direction Δz also affects the loss-of-correlation. It was already shown in Fig. 6 that any out-of-plane motion reduces F_O if not compensated by a parallel offset between the light sheets. Furthermore, for most flow examples, the out-of-plane velocity is not constant over the field of view and might change rapidly in space and time due to turbulence. To optimize measurements under these conditions, the light-sheet thickness, the optical magnification, and the time separation between the laser pulses must be tuned to obtain shift vector fields with sufficiently high displacement and a high valid detection probability. The sensitivity of the light-sheet profiles to a change in the out-of-plane motion $\partial_{\Delta z} F_O = \partial F_O / \partial \Delta z$ is an important parameter for this optimization. Figure 8 shows the rate of change of F_O with respect to Δz as a function of the light-sheet shape factor s for different initial out-of-plane motions.

Three important conclusions can be drawn from the figure: first, a Gaussian profile ($s = 2$) is much less sensitive to out-of-plan motion (or shot-to-shot beam pointing jitter) than a top-hat profile ($s \to \infty$). For perfectly aligned light sheets, $\partial_{\Delta z} F_O$ is close to zero in the case of a Gaussian, while it approaches -1 times the light-sheet thickness for top-hat profiles. Second, the mean out-of-plane motion Δz should be compensated by a light-sheet offset $\Delta z_{01} - \Delta z_{02}$, because the actual value of F_O decreases and its sensitivity to out-of-plane motion increases with the misalignment. Third, fluctuations in the out-of-plane motion due to turbulence or changes in the flow conditions must be limited by the time separation Δt between the two illuminations to minimize the loss-of-pairs. To ensure a high dynamic velocity range (Adrian 1997), it is recommended to allow for some spurious vectors which can be identified and replaced or rejected as long as they do not form clusters (Westerweel and Scarano 2005).

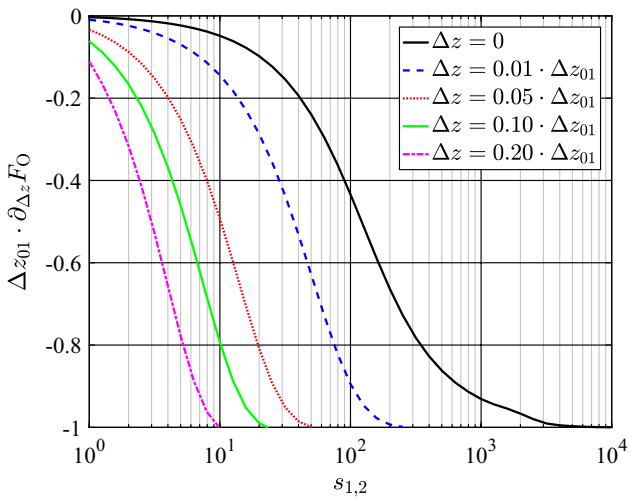

Fig. 8 Sensitivity of the loss-of-correlation with respect to the out-of-plane motion as a function of the light-sheet shape factor $s_{1,2}$ for different mean out-of-plane displacements Δz

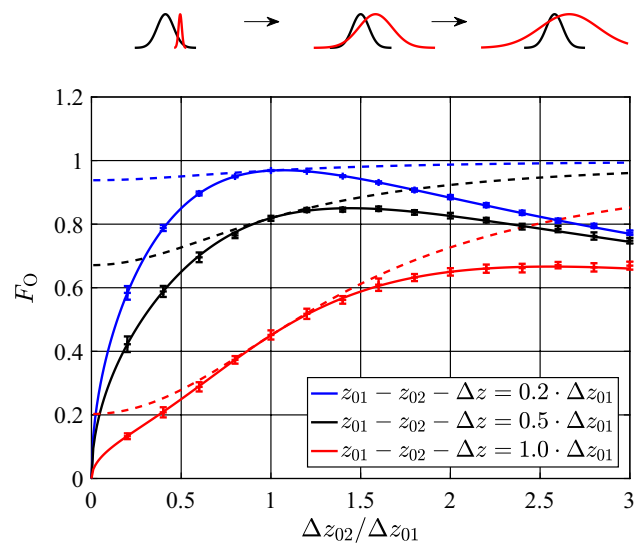

Fig. 9 Loss-of-correlation due to a parallel offset of the light sheets with respect to the out-of-plane motion $z_{01} - z_{02} - \Delta z$ can only be partially compensated by broadening one laser profile. The simulations are based on Gaussian profiles with a shape factor of $s_{1,2} = 2$. The dashed lines show the classical $F_{O(1992)}$ computed from Eq. (1)

Keane and Adrian (1992) suggested an optimization of the light-sheet width for the case of a parallel offset between the light sheets. In their work, it was stated that a sufficiently wide second light sheet ensures that all particle images from the first frame have partners in the second frame. Furthermore, they concluded that this condition is sufficient to achieve $F_O = 1$. This statement is misleading and needs to be discussed here.

Figure 9 illustrates how F_O changes if the width of the second light sheet is varied with respect to the first one for different parallel offsets between the light sheets. As before, the theoretical values according to Eq. (3) are shown together with the correlation height of synthetic images and the classical $F_{O(1992)}$ from Eq. (1). It is important to note that broadening the second light sheet does not compensate for the loss-of-correlation due to out-of-plane motion or light-sheet misalignment. This is due to the fact that the broader second light sheet also introduces new particle images which do not have partners in the first frame. The maxima of the curves in Fig. 9 are indeed shifted towards a broader width, but they never reach $F_O = 1$, as predicted by Keane and Adrian (1992). Larger $\Delta z_{01} - \Delta z_{02} - \Delta z$ offsets result in an optimum combination involving a lower F_O, as well as broader light sheets.

According to the classical definition of $F_{O(1992)}$ from Eq. (1), an infinitely wide second (Gaussian) light sheet fully compensates for an offset between the light sheets, indicated by the dashed lines in Fig. 9. This is not surprising, because the classical definition is not capable of correctly dealing with different light-sheet widths, as shown in Fig. 5. Furthermore, adjusting the width of just one of the two light sheets of a PIV laser is usually not feasible since it requires modifications to the intra-cavity optics.

6 Estimation of F_O using PIV correlation functions

After the establishment of a well-matched light-sheet baseline, the laser characteristics have been measured and quantified. Aided by this information, the influence of out-of-plane flow velocity components can now be considered on the PIV setup.

While a mean estimate of out-of-plane flow quantities can be used to approximate the necessary overlap adjustment required, this can be a relatively crude approach which also requires prior knowledge of the flow of interest. A more comprehensive approach to correcting for out-of-plane flow velocities involves an analysis of the PIV images captured from the experimental setup, which considers the cumulative impact of laser and out-of-plane velocity effects under non-zero and non-uniform in-plane displacements.

Under such non-uniform conditions, the correlation function broadens and its height decreases (Adrian 1988; Kähler and Scholz 2006; Scharnowski et al. 2012; Soria and Willert 2012). However, the volume of the (averaged) cross-correlation function remains constant if no loss-of-correlation or image noise is involved. The cross-correlation volume is equal to the volume of the averaged auto-correlation function and only depends on the particle image size. It is important to note that the loss-of-correlation factors due to in-plane-motion F_I (Adrian 1988) and in-plane gradients F_Δ (Westerweel 2008) both become unity for ideal measurements and state-of-the-art PIV data processing methods,

including multi-pass evaluation with iterative image deformation (Scarano 2001).

If out-of-plane motion is superimposed, the volume of the cross-correlation function is reduced, since some particle images do not have the corresponding partners, while the auto-correlation volume remains constant. The volume ratio is, therefore, equal to the F_O factor, as discussed in detail in Scharnowski and Kähler (2016a). The only known property that changes the volume of the auto-correlation function is image noise. In Scharnowski and Kähler (2016b), it was shown that the normalized auto-correlation function of noisy PIV images has a reduced correlation height that depends on the image noise level and the standard deviation of the noise-free image intensity. Only the center peak height equals one due to the self-correlation of the image noise. The loss-of-correlation due to image noise F_σ can be estimated by determining the auto-correlation function's height from a fit function that excludes the center peak, according to Scharnowski and Kähler (2016b).

Fortunately, image noise also reduces the volume of the cross-correlation function by the same amount. Thus, in addition to the findings in Scharnowski and Kähler (2016a), F_O can now also be estimated using noisy PIV images by computing the ratio of the cross-correlation volume V_C and the auto-correlation volume V_R^*. In this calculation, the auto-correlation center peak is replaced by a fitted value:

$$F_O = \frac{V_C}{V_R^*}. \tag{4}$$

In Scharnowski and Kähler (2016a), it was shown that F_O can be estimated reliably using this technique for a broad range of different conditions, e.g., various light-sheet shape factors, particle image diameters, and displacement fluctuations. To demonstrate that Eq. (4) is also suited for noisy PIV images, Fig. 10 shows the estimated F_O [calculated using Eq. (4)] with respect to the simulated F_O for different noise levels. The symbols and the error bars in the figure represent the mean volume ratio and its standard deviation computed from 1000 correlation function pairs, respectively. An interrogation window size of 64×64 pixel was used and the inner 17×17 pixel around the center (without the center peak for the auto-correlation) was approximated by a Gaussian fit function. The results show good agreement with the theory. The volume ratio only begins to overestimate the loss-of-correlation factor when $F_O < 0.3$. However, measurements with $F_O < 0.3$ will not lead to reliable results, so this deviation is not at all important in practice.

The uncertainty of F_O estimated using the volume ratio depends on particle image density and the interrogation window size, since a smooth correlation function is required for the fitting procedure. Figure 11 shows the standard deviation

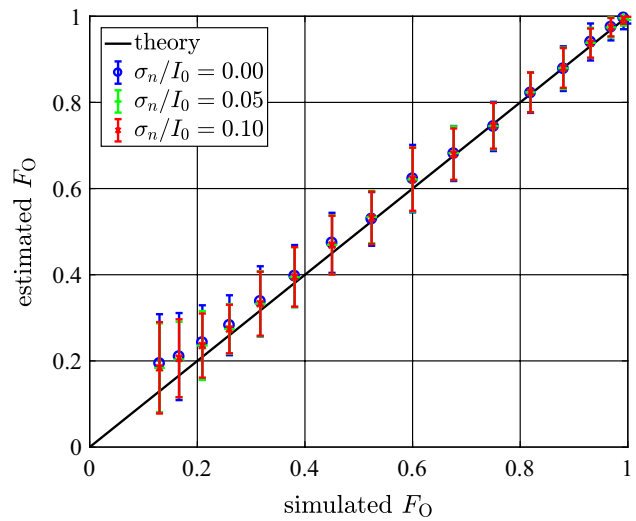

Fig. 10 Estimated F_O based on the volume ratio in Eq. (4) versus the simulated F_O computed from Eq. (3) for different image noise levels

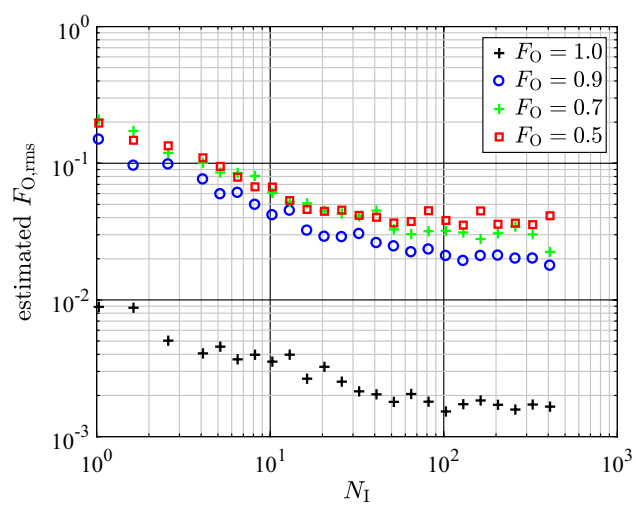

Fig. 11 Uncertainty of the estimated loss-of-correlation versus average number of particle images per interrogation window for different F_O

of the estimated F_O with respect to the average number of particle images N_I within a 64×64 pixel interrogation window. Different out-of-plane displacements are tested using synthetic PIV images. Two conclusions can be drawn from the figure: First, the uncertainty is rather independent of F_O in the range $0.5 \leq F_O \leq 0.9$ and decreases rapidly for values approaching $F_O = 1$. Second, increasing the particle image density reduces the uncertainty of the estimated F_O until a significant amount of particle images start to overlap. It can be concluded that F_O is estimated reliably from the correlation–function volume ratio if the interrogation window size is large enough to contain about 100 particle images.

The use of the correlation–function volume ratio to estimate F_O, unlike isolated profiling of the light sheet, incorporates all of the out-of-plane loss-of-pairs variables captured in PIV images. In addition, the increased robustness of advanced image correlation algorithms to spurious vectors mean that such outliers may not always be present in PIV data as an indicator for correlation quality. Calculation of F_O using the correlation–function volume ratio can, therefore, offer a more detailed assessment of correlation quality to inform experimentalists. Furthermore, this technique can be applied retrospectively to previous PIV datasets to quantify F_O, and help troubleshoot and isolate any causes of degradation in PIV results throughout an experiment. However, correct refinement and measurement of a well-matched light-sheet baseline using a laser profiling camera (or similar profiling technique) can be of use prior to the correlation–function volume ratio calculation, to avoid the guess-and-check iteration encountered when attempting to improve F_O without substantive guidance and feedback.

7 Experimental validation

A 2D, two-pulse PIV experiment was performed to further investigate the impacts of various laser light-sheet mismatch scenarios under laboratory conditions, and demonstrates the experimental estimation of F_O. Turbulent boundary layer measurements at $Re_\theta \approx 7500$ were captured over a streamwise–spanwise plane in the High Reynolds Number Boundary Layer Wind Tunnel (HRNBLWT) at the University of Melbourne (see Nickels et al. 2005 for further details concerning this facility). The measurement was performed at a wall normal height of approximately 240 viscous units (corresponding to ≈ 10 mm) and extended over a region of 4200 × 6300 viscous units (streamwise × spanwise, corresponding to 175 mm × 265 mm). Further details regarding this experimental setup configuration and measurement procedure can be found in de Silva et al. (2015) and Grayson et al. (under review) respectively. In summary, a 10.7 megapixel PCO 4000 PIV camera with a Nikon AF Micro-Nikkor 60 mm 2.8D lens was used for image capture, achieving a flow resolution of approximately 1.6 viscous units/pixel. Polyamide particles were used for seeding, and the measurement plane was illuminated by a Spectra-Physics Quanta-Ray PIV-400 532 nm Nd:YAG pulsed laser (nominally at 400 mJ per pulse), a system which allows easy access to the beam combining optics. Adjustments to the combining optics allow the light-sheet mismatch to be modified, enabling an examination of the associated impacts on measurement results.

Eight distinct light-sheet mismatch scenarios were measured, where light-sheet overlap was adjusted via the laser's beam combining optics. A set of 120 PIV image pairs were captured for each mismatch case, in addition to profiles of the light sheet using a beam profiling camera (see Grayson et al. 2016, Grayson et al. under review). A temporal separation between the laser pulses of $\Delta t = 110$ µs was used in these measurements, leading to a mean displacement of ≈ 11 pixel, or 0.7 mm in the streamwise direction. Image pairs were processed using state-of-the-art multi-pass PIV evaluation software, including image deformation and Gaussian window weighting with a final interrogation window size of 32^2 pixel and an overlap of 50%. Figure 12 (*left*) shows a sample flow field under one of the measured misalignment scenarios (the flow direction is from left to right), where color contours indicate the streamwise velocity. The instantaneous flow field exhibits elongated coherent structures of different velocities which extend along the streamwise direction.

Figure 12 (*right*) shows the corresponding instantaneous distribution of F_O estimated from the volume ratio of Eq. (4) using 128^2 pixel interrogation windows with 50% overlap. A general trend of decreasing F_O from top to bottom is clearly visible in the figure. Although optical camera effects and seeding also play a role, this trend is primarily caused by a decreasing overlap of the light sheets from top to bottom, as shown in Fig. 13 for three y locations of the field of view.

Moreover, the F_O distribution in Fig. 12 (*right*) features local fluctuations which are caused by loss-of-pairs due to out-of-plane motion. At $70 \leq y \leq 80$mm for example, a turbulent flow structure of low momentum (dark blue in Fig. 12 on the left) causes an increase in F_O from ≈ 0.6 to values above 0.9. In this region, fluid is transported away

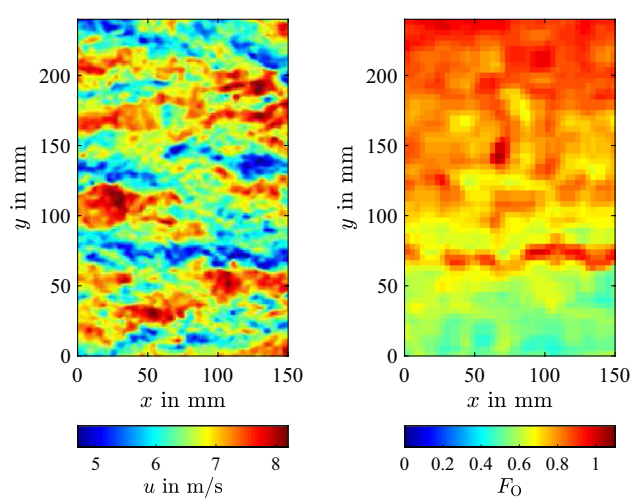

Fig. 12 Example of the instantaneous distribution of the streamwise velocity in a wall-parallel plane of a turbulent boundary layer (left) and the corresponding F_O estimated from the correlation volume ratio (right). The light-sheet profiles were intentionally misaligned to study the effect of F_O on the velocity estimation (Grayson et al. 2016, Grayson et al. under review). The measured light-sheet profiles are shown in Fig. 13 for three spanwise locations

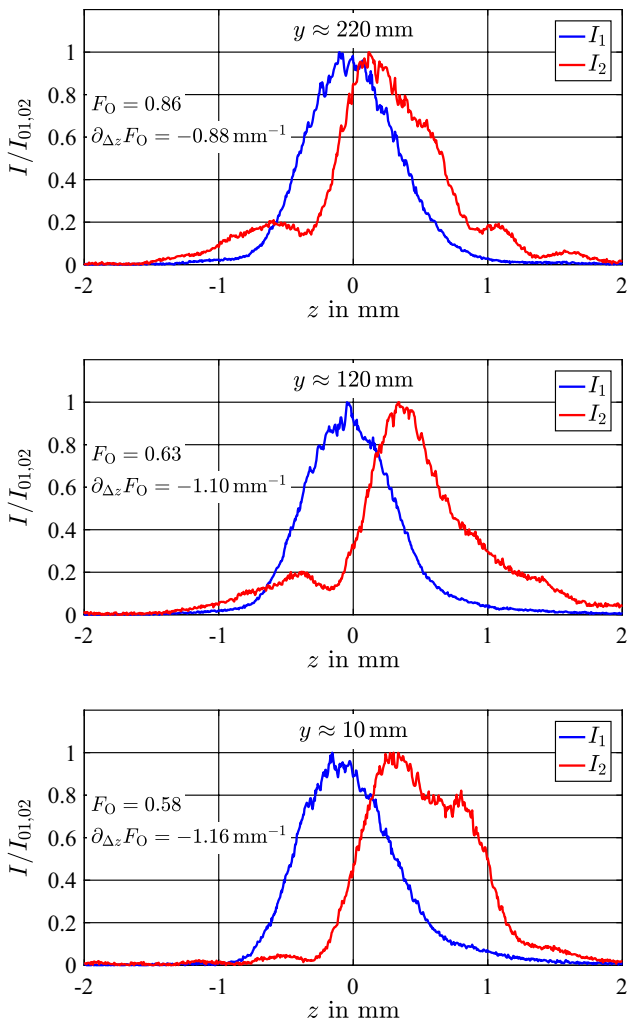

Fig. 13 Light-sheet intensity profiles for three different spanwise locations corresponding to the PIV measurements shown in Fig. 12

from the wall and the out-of-plane motion of the particles is partly compensated by the offset between the light sheets (see Fig. 13). In other regions, F_O is reduced due to motion of the particles towards the wall. Nevertheless, with a particle image density of $N_{ppp} \approx 0.03$, the valid vector detection probability is close to 100% for $F_O > 0.5$, as illustrated in Fig. 1. If the resolution needs to be improved by reducing the interrogation window size, the light-sheet overlap must be optimized.

Figure 14 illustrates how the interrogation window size affects the estimation of the velocity fluctuations. While similar behaviors are observed using 64^2 pixel and 32^2 pixel windows (apart from small deviations close to $y = 0$), the estimated velocity fluctuations from smaller 16^2 pixel windows deviate from the larger interrogation window estimates across the lower half of the field of view. The 16^2 pixel window fluctuations estimate reaches values almost three times higher than for the larger window sizes. This was to

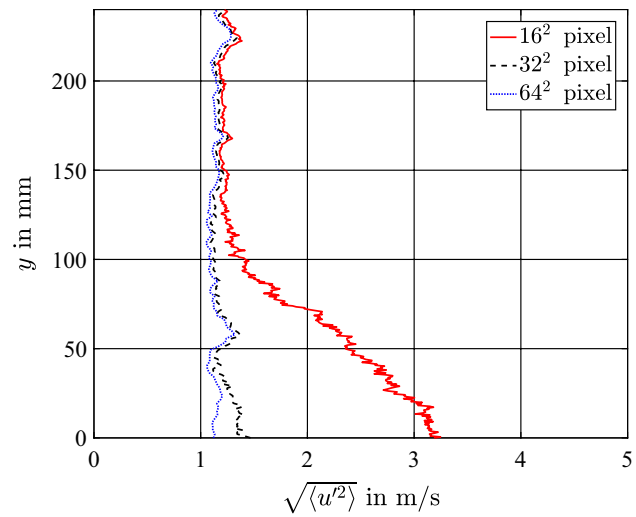

Fig. 14 Estimated streamwise velocity fluctuations as a function of the spanwise location for different interrogation window sizes. The light-sheet overlap decreases for decreasing y, as shown in Fig. 13

be expected, because the number of paired particle images found within the small interrogation windows is too low to guarantee valid vectors with low uncertainty under strong light-sheet misalignment conditions.

This example shows that knowledge about the light-sheet intensity profile and alignment help experimentalists to understand what exactly causes the loss-of-correlation and how the results could be improved. The alignment can be easily seen from a laser profiling camera (Grayson et al. 2016), but is also indirectly assessable using the correlation–function volume ratio. Figure 15 shows that both

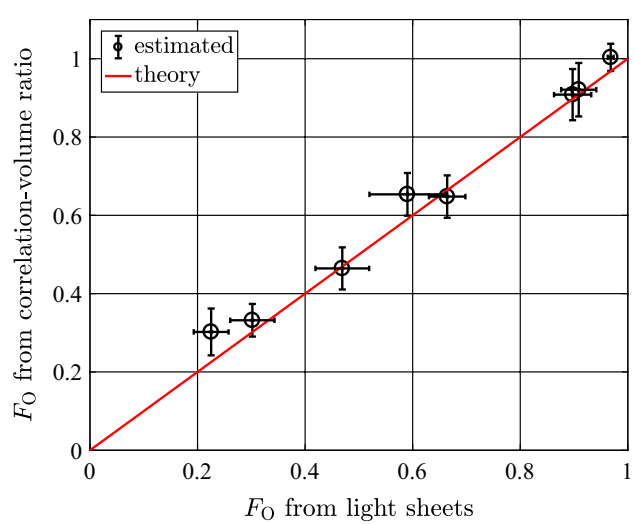

Fig. 15 Estimated F_O from PIV experiments based on the correlation function volume ratio of Eq. (4) compared with the estimation of F_O from the light-sheet profiles according to Eq. (3)

methods result in a fairly good agreement over the broad range of laser sheet mismatch scenarios. The combination of both methods allows for an easy alignment of the lasers prior the experiment by means of a profiling camera, and readjustments in the presence of a mean out-of-plane motion by using the correlation–function volume ratio. The latter method also allows the detection of changes in F_O due to fluctuations in the out-of-plane motion. This analysis not only confirms the theoretical findings of the previous sections, but also substantiates the value and utility of the F_O metric to characterize and improve the quality of a PIV measurement.

8 Summary and discussion

A new definition for the loss-of-correlation due to out-of-plane effects is proposed in this work with the aim to generalize the classical definition of F_O by Keane and Adrian (1992). While the classical definition only works for the case of identical light-sheet profiles, the new definition is also suited for light sheets which differ in intensity distribution and width.

The comparison of different light-sheet scenarios revealed that a parallel offset between the light sheets or an out-of-plane motion has the strongest impact on the loss-of-correlation (see Fig. 6). In addition, a difference in the width can cause significant reduction in the correlation strength, as shown in Fig. 5. On the other hand, if the width of both light sheets is comparable, the shape has only minor impact on F_O (see Fig. 4). The classical definition from Keane and Adrian (1992) in Eq. (1) only continues to hold for light sheets with the same shape.

Based on the new definition, F_O can be estimated reliably from laser profiles in the case of zero out-of-plane motion. Furthermore, it was demonstrated that the ratio of the cross-correlation function and the auto-correlation function provides F_O directly from PIV images. Thus, an online optimization of the PIV setup is easily possible for flows with out-of-plane motion.

The findings of this work allow PIV users to optimize their experiment with respect to the loss-of-correlation due to out-of-plane effects. Furthermore, the results can assist the selection of suitable PIV lasers based on the beam profiles. The analysis implies that the quality of the laser beams are important and therefore care must be taken when buying lasers for flow field investigations.

References

Adrian RJ (1988) Double exposure, multiple-field particle image velocimetry for turbulent probability density. Opt Laser Eng 9:211–228. doi:10.1016/S0143-8166(98)90004-5

Adrian RJ (1997) Dynamic ranges of velocity and spatial resolution of particle image velocimetry. Meas Sci Technol 8:1393. doi:10.1088/0957-0233/8/12/003

Charonko JJ, Vlachos PP (2013) Estimation of uncertainty bounds for individual particle image velocimetry measurements from cross-correlation peak ratio. Meas Sci Technol 24(6):065301. doi:10.1088/0957-0233/24/6/065301

de Silva CM, Squire DT, Hutchins N, Marusic I (2015) Towards capturing large scale coherent structures in boundary layers using particle image velocimetry. In: 7th Australian conference on laser diagnostics in fluid mechanics and combustion, Melbourne, Australia, 9–11 Dec 2015

Fond B, Abram C, Beyrau F (2015) On the characterisation of tracer particles for thermographic particle image velocimetry. Appl Phys B 118(3):393–399

Ganapathisubramani B, Longmire EK, Marusic I, Pothos S (2005) Dual-plane PIV technique to determine the complete velocity gradient tensor in a turbulent boundary layer. Exp Fluids 39(2):222–231. doi:10.1017/S0022112004002277

Grayson K, de Silva CM, Hutchins N, Marusic I (2016) Laser light sheet profile and alignment effects on PIV performance. In: 18th international symposium on applications of laser and imaging techniques to fluid mechanics, Lisbon, Portugal, 4–7 July 2016

Grayson K, de Silva CM, Hutchins N, Marusic I (2017) Beam stability and warm-up effects of Nd: YAG lasers used in particle image velocimetry. Meas Sci Technol 28(6):065301

Grayson K, de Silva CM, Hutchins N, Marusic I (under review) Impact of mismatched and misaligned laser light sheet profiles on PIV performance. Exp Fluids

Kähler CJ, Kompenhans J (2000) Fundamentals of multiple plane stereo PIV. Exp Fluids 29:70–77. doi:10.1007/s003480070009

Kähler CJ, Scholz U (2006) Transonic jet analysis using long-distance micro PIV. In: 12th international symposium on flow visualization, Göttingen, Germany, 10–14 Sept 2006

Kähler CJ, Adrian RJ, Willert CE (1998) Turbulent boundary layer investigations with conventional and stereoscopic particle image velocimetry. In: 9th international symposium on applications of laser techniques to fluid mechanics, Lisbon, Portugal, 13–16 July 1998

Kähler CJ, Scharnowski S, Cierpka C (2012) On the uncertainty of digital PIV and PTV near walls. Exp Fluids 52:1641–1656. doi:10.1007/s00348-012-1307-3

Keane RD, Adrian RJ (1992) Theory of cross-correlation analysis of PIV images. Appl Sci Res 49:191–215. doi:10.1007/BF00384623

Mistry D, Dawson J (2014) Experimental investigation of multi-scale entrainment processes of a turbulent jet. In: 17th international symposium on applications of laser techniques to fluid mechanics, Lisbon, Portugal, 7–10 July 2014

Nickels TB, Marusic I, Hafez S, Chong MS (2005) Evidence of the -1-law in a high-Reynolds-number turbulent boundary layer. Phys Rev Lett 95(7):074501

Scarano F (2001) Iterative image deformation methods in PIV. Meas Sci Technol 13:R1–R19. doi:10.1088/0957-0233/13/1/201

Scharnowski S, Kähler CJ (2016a) Estimation and optimization of loss-of-pair uncertainties based on PIV correlation functions. Exp Fluids 57:23. doi:10.1007/s00348-015-2108-2

Scharnowski S, Kähler CJ (2016b) On the loss-of-correlation due to PIV image noise. Exp Fluids 57:119. doi:10.1007/s00348-016-2203-z

Scharnowski S, Hain R, Kähler CJ (2012) Reynolds stress estimation up to single-pixel resolution using PIV-measurements. Exp Fluids 52:985–1002. doi:10.1007/s00348-011-1184-1

Sciacchitano A, Wieneke B (2016) PIV uncertainty propagation. Meas Sci Technol 27(8):084006. doi:10.1088/0957-0233/27/8/084006

Sciacchitano A, Neal DR, Smith BL, Warner SO, Vlachos PP, Wieneke B, Scarano F (2015) Collaborative framework for PIV uncertainty quantification: comparative assessment of methods. Meas Sci Technol 26:074004. doi:10.1088/0957-0233/26/7/074004

Soria J, Willert C (2012) On measuring the joint probability density function of three-dimensional velocity components in turbulent flows. Meas Sci Technol 23:065301. doi:10.1088/0957-0233/23/6/065301

Timmins BH, Wilson BW, Smith BL, Vlachos PP (2012) A method for automatic estimation of instantaneous local uncertainty in particle image velocimetry measurements. Exp Fluids 53(4):1133–1147. doi:10.1007/s00348-012-1341-1

Westerweel J (2008) On velocity gradients in PIV interrogation. Exp Fluids 44:831–842. doi:10.1007/s00348-007-0439-3

Westerweel J, Scarano F (2005) Universal outlier detection for PIV data. Exp Fluids 39:1096–1100. doi:10.1007/s00348-005-0016-6

Wieneke B (2015) PIV uncertainty quantification from correlation statistics. Meas Sci Technol 26(7):074002. doi:10.1088/0957-0233/26/7/074002

Xue Z, Charonko JJ, Vlachos PP (2015) Particle image pattern mutual information and uncertainty estimation for particle image velocimetry. Meas Sci Technol 26(7):074001